J|A|C|S
ARTICLES

Published on Web 03/13/2009

Controllable Epitaxial Crystallization and Reversible Oriented Patterning of Two-Dimensional Colloidal Crystals

Rongguo Xie and Xiang-Yang Liu*

Department of Physics, National University of Singapore, 2 Science Drive 3, Singapore 117542

Received January 5, 2009; E-mail: phyliuxy@nus.edu.sg

Abstract: We demonstrate a reliable and highly efficient epitaxial templating approach for the formation of two-dimensional (2D) colloidal crystals. By applying an alternating electric field (AEF), one-dimensional colloidal lines are used as an epitaxial template to site specifically initiate 2D colloidal crystallization and control the orientation of the 2D colloidal crystals. The kinetics of the crystallization and structure ordering is precisely and conveniently manipulated by the external AEF. The well-defined artificial linear defects are embedded inside the 2D colloidal crystals by means of heteroepitaxy, whereas the unwanted existing defects are controllably relaxed via an electrically induced annealing process. This epitaxial templating approach is fast, reversible, and amenable for large-area oriented patterning of colloidal crystals, providing a new way for the creation of novel materials and devices with functions and properties that can be reversibly changed, such as electrically tunable photonic waveguides and e-papers.

1. Introduction

The self-assembly and fabrication of two- or three-dimensional (2D/3D) colloidal crystals have attracted broad interest for many potential applications, such as photonic crystals,[1−4] chemical and biochemical sensors,[5,6] optoelectronic devices[7,8] and templates for colloidal nanolithgraphy.[9] In order to achieve practical applications, two major obstacles need to be overcome. First, many applications for colloidal crystals require samples which are free from defects over large length scales. However, most self-assembly systems suffer from disorders resulting from homogeneous nucleation and uncontrollable crystal growth. For instance, point defects and grain boundaries are difficult to avoid in 2D colloidal crystals. Several controlled assembly methods, such as growing crystals with a template[10−13] and in a temperature gradient[14] have been developed to combat these disorders. However, these methods involve a slow and complicated process or still produce a large number of intrinsic defects. An alternative approach to minimize defect density is to remove defects after the crystal has self-assembled. Unfortunately, thermal cycling, which is commonly used to anneal atomic and molecular solids, cannot be applied to colloidal crystals in general, because the free-energy barriers to collective rearrangements are often large.[15,16] Second, the introduction of well-defined artificial defects within colloidal crystals is another prerequisite for some practical applications.[17] Linear defects, for instance, could be used as photonic waveguides and point defects as microcavities.[7] However, this cannot be achieved through conventional self-assembly methods alone, as the intentionally added defects will substantially frustrate the crystal growth and locally induce disordering in colloidal crystals.[18] Experimentally, a significant challenging issue for practical applications of colloidal crystals has been a lack of reliable and easily controlled methods for crystallization of the colloidal particles into large, perfect single crystals with predefined orientations, artificial defects, and patterns over fast time scales.

In this work, we demonstrate a reliable and rapid epitaxial templating approach for the controllable crystallization of large-area 2D colloidal crystals with well-defined orientations, artificial defects, and patterns. We show that predefined 1D colloidal lines can be utilized to site specifically initiate the 2D colloidal nucleation and control the crystal orientation, wherein an external alternating electric field (AEF) allows us to precisely and conveniently manipulate the kinetic process of the crystal growth. We conduct real-time direct observation and quantitative measurements to reveal the epitaxial ordering mechanism. This epitaxial templating approach enables unprecedented control

(1) Wijnhoven, J. E. G. J.; Vos, W. L. *Science* **1998**, *281*, 802.
(2) Norris, D. J.; Vlasov, Y. A. *Adv. Mater.* **2001**, *13*, 371.
(3) Vlasov, Y. A.; Bo, X. Z.; Sturm, J. C.; Norris, D. J. *Nature* **2001**, *414*, 289–293.
(4) Hynninen, A.-P.; Thijssen, J. H. J.; Vermolen, E. C. M.; Dijkstra, M.; van Blaaderen, A. *Nat. Mater.* **2007**, *6*, 202–205.
(5) Holtz, J. H.; Asher, S. A. *Nature* **1997**, *389*, 829–832.
(6) Velev, O. D. E.; Kaler, W. *Langmuir* **1999**, *15*, 3693.
(7) Joannopoulos, J. D.; Villeneuve, P. R.; Fan, S. *Nature* **1997**, *386*, 143–149.
(8) Yamasaki, T.; Tsutsui, T. *Appl. Phys. Lett.* **1998**, *72*, 1957.
(9) Yang, S. M.; Jang, S. G.; Choi, D. G.; Kim, S.; Yu, H. K. *Small* **2006**, *2*, 458–475.
(10) van Blaaderen, A.; Ruel, R.; Wiltzius, P. *Nature* **1997**, *385*, 321–324.
(11) Yin, Y. D.; Xia, Y. N. *Adv. Mater.* **2002**, *14*, 605.
(12) Kumacheva, E.; Garstecki, P.; Wu, H. K.; Whitesides, G. M. *Phys. Rev. Lett.* **2003**, *91*, 128301.
(13) Winkleman, D.; Gates, B. D.; McCarty, L. S.; Whitesides, G. M. *Adv. Mater.* **2005**, *17*, 1507.
(14) Cheng, Z. D.; Russel, W. B.; Chaikin, P. M. *Nature* **1999**, *401*, 893–895.
(15) Wei, Q. H.; Cupid, D. M.; Wu, X. L. *Appl. Phys. Lett.* **2000**, *77*, 1641–1643.
(16) Korda, P. T.; Grier, D. G. *J. Chem. Phys.* **2001**, *114*, 7570–7543.
(17) Arsenault, A.; Fleischhaker, F.; von Freymann, G.; Kitaev, V.; Miguez, H.; Mihi, A.; Tétreault, N.; Vekris, E.; Manners, I.; Aitchison, S.; Perovic, D.; Ozin, G. A. *Adv. Mater.* **2006**, *18*, 2779–2885.
(18) de Villeneuve, V. W. A.; Dullens, R. P. A.; Aarts, D. G. A. L.; Groeneveld, E.; Scherff, J. H.; Kegel, W. K.; Lekkerkerker, H. N. W. *Science* **2005**, *309*, 1231–1233.

10.1021/ja900049r CCC: $40.75

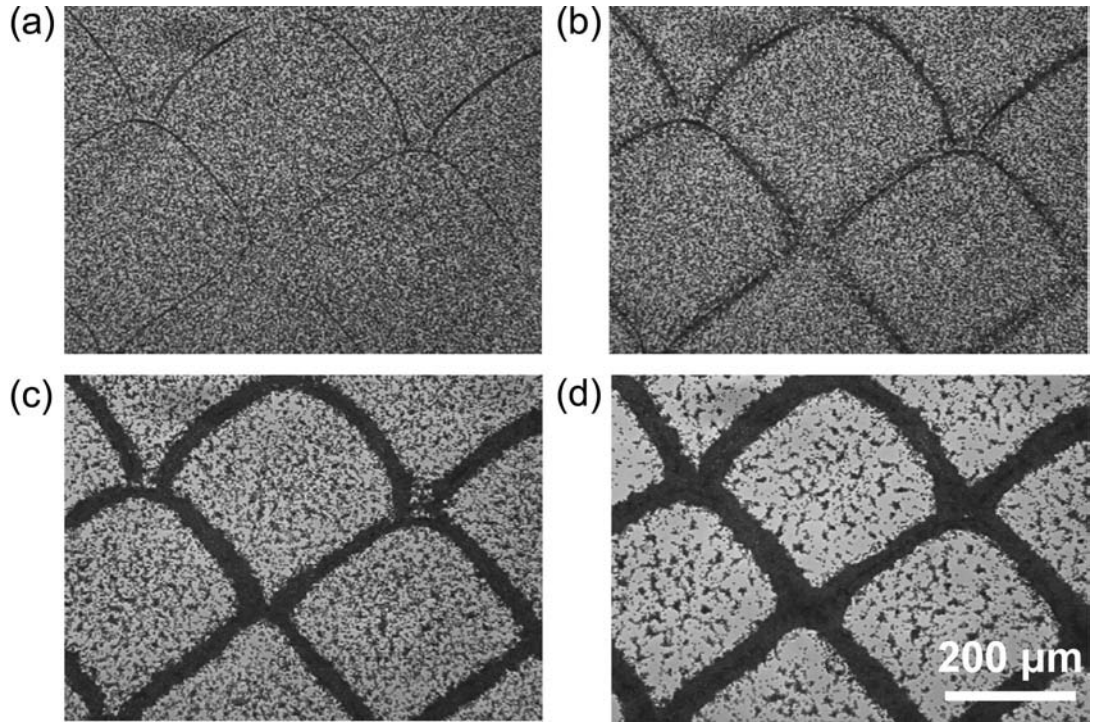

Figure 1. Time snapshots of large-area epitaxial crystallization and oriented patterning of a 2D colloidal crystal using a colloidal line network as a template, under the AEF of frequency $f = 400$ Hz and field strength $E_0 = 4.0 \times 10^4$ V/m. (a) 0 s, (b) 2.0 s, (c) 5.0 s, (d) 10.0 s.

over the defects inside the 2D colloidal crystals and large-area electrically reversible patterning of 2D colloidal crystals, thus expanding the potential for a wide range of practical applications, such as electrically tunable photonic waveguides and e-papers.[19]

2. Results and Discussion

Figure 1 shows a typical process of large-area epitaxial crystallization and patterning of 2D colloidal crystals using a prepatterned colloidal-line network as a template. (Digital video of the process is available in Supporting Information Video 1.) Initially, an aqueous dispersion of 1.8 μm colloidal particles was sandwiched and sealed in a cell composed of two parallel ITO electrodes; colloidal lines with a predesigned network pattern composed of 1.8 μm colloidal particles were deposited on the bottom ITO electrode using a confined dewetting lithography method[20] (Figure 1a, $t = 0$ s). Upon application of the AEF of frequency $f = 400$ Hz and field strength $E_0 = 4.0 \times 10^4$ V/m, the freely dispersed colloidal particles in the bulk fluid phase were transported to the electrode surface and accumulated near the colloidal lines directed by the electric-field-induced fluid flows.[21−33] Heterogeneous nucleation occurred first at the template due to a lowering of nucleating barriers,[34] which site specifically initiated the epitaxial crystallization of the colloidal particles (Figure 1b, $t = 2.0$ s). Subsequently, some homogeneous nuclei were formed in the bulk fluid phase when they overcame a homogeneous nucleation barrier (Figure 1c, $t = 5.0$ s). The colloidal crystal initiated at the template kept on growing, whereas the growth units in the bulk fluid phase, such as dimer, trimer, and the homogeneous nuclei, were transported toward the growing front of the templated colloidal crystal (Figure 1d, $t = 10$ s). Eventually when all the colloidal particles in the bulk fluid phase have been assembled at the template, the colloidal crystal stopped growing, forming a colloidal crystal network with the pattern reproduced from the template.

This novel epitaxial templating process offers several distinct advantages above other methods currently in use. First, tuning frequency of the AEF provides a reliable and convenient tool to precisely manipulate the crystallization conditions externally. Second, the assembly/disassembly process is fully reversible on turning on/off of the AEF. Third, it is very rapid; the time scale for the crystallization is only tens of seconds. These advantages make it feasible to quantitatively study the crystal growth kinetics in a single sample for many times and to quickly screen the optimal crystallization conditions for generating high-quality colloidal crystal patterns. In the following, we conduct

(19) Comiskey, B.; Albert, J. D.; Yoshizawa, H.; Jacobson, J. *Nature* **1998**, *394*, 253–255.
(20) Celio, H.; Barton, E.; Stevenson, K. J. *Langmuir* **2006**, *22*, 11426–11435.
(21) Trau, M.; Saville, D. A.; Aksay, I. A. *Science* **1996**, *272*, 706–709.
(22) Trau, M.; Saville, D. A.; Aksay, I. A. *Langmuir* **1997**, *13*, 6375–6381.
(23) Sides, P. J. *Langmuir* **2003**, *19*, 2745–2751.
(24) Nadal, F.; Argoul, F.; Hanusse, P.; Pouligny, B. *Phys. Rev. E* **2002**, *65*, 061409–061416.
(25) Ristenpart, W. D.; Aksay, I. A.; Saville, D. A. *Phys. Rev. E* **2004**, *69*, 021405–021412.
(26) Fagan, J. A.; Sides, P. J.; Prieve, D. C. *Langmuir* **2006**, *22*, 9846–9852.
(27) Hoggard, J. D.; Sides, P. J.; Prieve, D. C. *Langmuir* **2007**, *23*, 6983–6990.
(28) Zhang, K. Q.; Liu, X. Y. *Nature* **2004**, *429*, 739–743.
(29) Zhang, T. H.; Liu, X. Y. *J. Phys. Chem. C* **2007**, *111*, 1342–1346.
(30) Zhang, K. Q.; Liu, X. Y. *Appl. Phys. Lett.* **2007**, *90*, 111911.
(31) Liu, Y.; Xie, R. G.; Liu, X. Y. *Appl. Phys. Lett.* **2007**, *91*, 063105.
(32) Xie, R. G.; Liu, X. Y. *Appl. Phys. Lett.* **2008**, *92*, 083106.
(33) Xie, R. G.; Liu, X. Y. *Adv. Funct. Mater.* **2008**, *18*, 802–809.
(34) Cacciuto, A.; Auer, S.; Frenkel, D. *Nature* **2004**, *428*, 404–406.

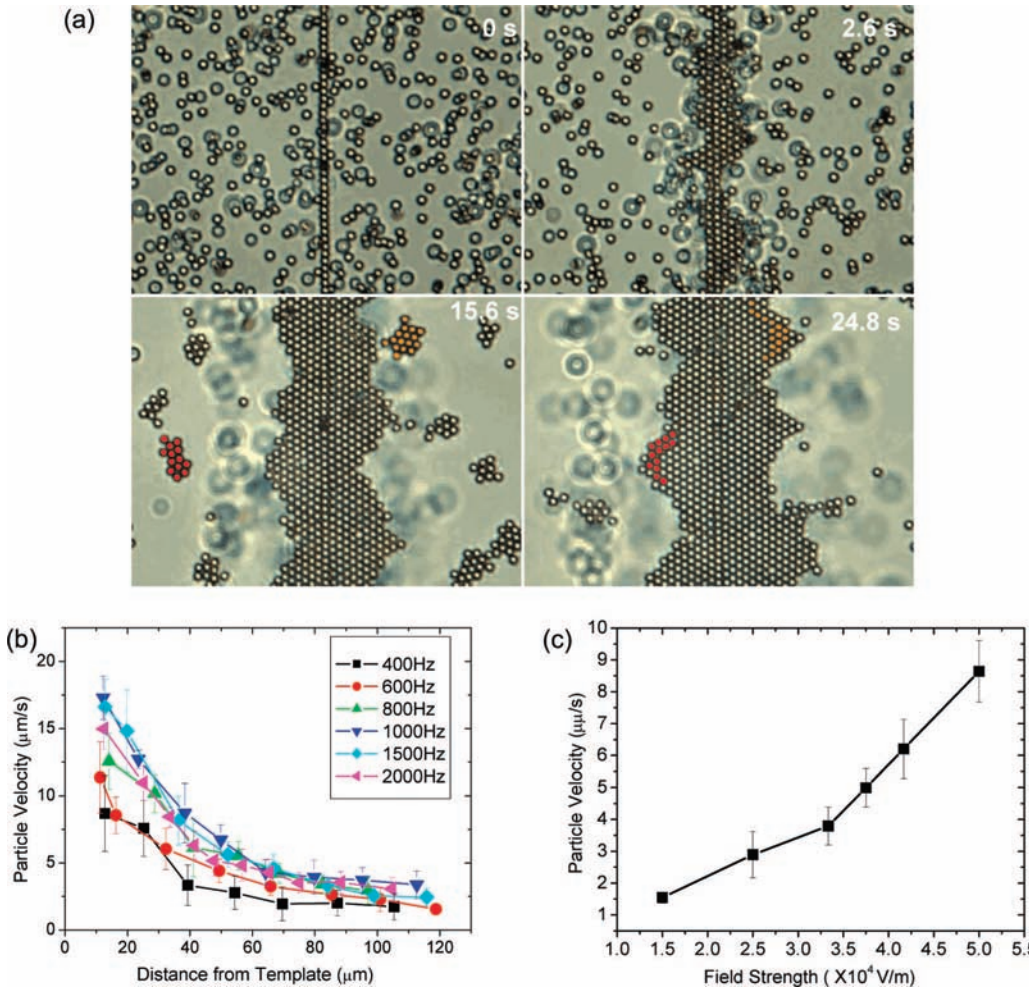

Figure 2. (a) Time snapshots of the epitaxial crystallization of 1.8 μm colloidal particles using a 1.8 μm colloidal line as a template, under the AEF of frequency $f = 800$ Hz and field strength $E_0 = 4.0 \times 10^4$ V/m. The bright dots correspond to the well-focused particles that are assembled on the bottom electrode. The dark dots correspond to the ill-focused spheres, which are suspended in the bulk solution. (b) Particle velocity as a function of distance from the colloidal line for different frequencies. (c) Particle velocity as a function of field strength at a fixed distance of 10 μm from the colloidal line at 400 Hz at a fixed field strength $E_0 = 4.0 \times 10^4$ V/m.

real-time and real-space observations at single-particle level to systematically study the epitaxial ordering mechanism by varying the frequency and the field strength of the AEF, wherein single straight colloidal lines are used as a model template.

Figure 2a shows the direct observation of the epitaxial crystallization and time evolution of some nuclei. (Digital video of the process is available in Supporting Information Video 2.) A single, straight colloidal line composed of 1.8 μm colloidal particles was used as a template to match the size of the crystallizing colloidal particles (Figure 2a, $t = 0$ s). Upon the application of the AEF of frequency $f = 800$ Hz and field strength $E_0 = 4.0 \times 10^4$ V/m, rapid 2D colloidal epitaxial crystallization dynamically nucleated a large number of separate islands at the template (Figure 2a, $t = 2.6$ s), showing a remarkable resemblance to the Volmer−Weber island growth mode[35] in atomistic epitaxy process. Subsequently, homogeneous nuclei were randomly formed in the bulk fluid phase, as shown in Figure 2a ($t = 15.6$ s) and then were transported toward the growing front at the template. During the incorporation process, the downward funneling (DF) effect[35] was observed: particles deposited beyond an island edge would funnel down to the lowest positions in the vicinity of the deposition site (see the Supporting Information, Video 2). The evolution of two typical homogeneous nuclei is highlighted by the red and yellow particles in Figure 2a, respectively. Although these homogeneous nuclei were randomly oriented in the bulk fluid phase ($t = 15.6$ s, and $t = 24.8$ s), they would rearrange themselves to find their optimal positions and orientations when they deposited on the islands, forming a single colloidal crystal with a well-defined orientation with respect to the colloid line. Figure 2b shows the particle velocity as a function of distance to the template at different frequencies at a fixed field strength $E_0 = 4.0 \times 10^4$ V/m, showing that the incoming particles were strongly accelerated as they approached the growing front. The acceleration of incoming particles serves as strong evidence of the existence of long-range attractions between the template and the incoming particles. The long-range (120 ± 20 μm) nature suggests that these attractions are driven by electrohydrodynamic (EHD) flows generated by the gradient of the electric field.[21−33] Figure 2c shows the particle arrival velocity (measured at 10 μm from the template) as a function of the field strength. The particle velocity increased with increasing the field strength, which is consistent with the EHD model.[21−33] Note that the epitaxial crystallization process involves two kinds of EHD

(35) Herman, M. A.; Richter, W.; Sitter, H. *Epitaxy: Physical Principles and Technical Implementation*; Springer: Berlin, 2004.

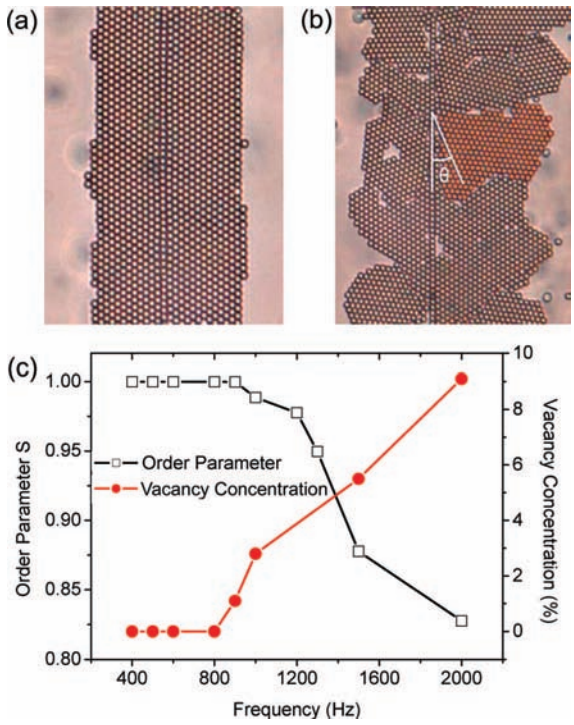

Figure 3. (a and b) Optical images of the templated colloidal crystals composed of 1.8 μm colloidal particles obtained under the AEF of different frequency at a fixed field strength $E_0 = 4.0 \times 10^4$ V/m and (a) $f = 800$ Hz or (b) $f = 2000$ Hz. (c) Orientational order parameter S and vacancy concentration of the colloidal crystals as a function of frequency f. The field strength was fixed at $E_0 = 4.0 \times 10^4$ V/m.

attractions. The first originates from the colloidal line template, which distorts the local electric filed and sets up the long-range attractions between the template and the incoming particles. This kind of EHD attraction transports the growth units far away from the template to the growing front. The second acts among the mobile particles in the bulk fluid phase, and is generated by the gradients in current density caused by the presence of these particles near the electrode surface.[21−33] This kind of attraction enables the particles to overcome the induced repulsive dipole−dipole interactions and locally assemble the colloidal particles into the ordered crystalline structures above the electrode surface in the bulk liquid phase.

The degree of perfection of the colloidal crystals changes with the frequency of the AEF. Figure 3, panels a and b, show two typical images of the colloidal crystals formed at the same template at $f = 800$ Hz and $f = 2000$ Hz, respectively. The field strength was fixed at $E_0 = 4.0 \times 10^4$ V/m. As can be seen, a single crystal with a well-defined orientation with respect to the template was obtained at $f = 800$ Hz, whereas a polycrystalline crystal containing randomly oriented domains and a large number of vacancies was formed at $f = 2000$ Hz. To characterize the effect of frequency on the epitaxial ordering, the orientational order parameter[36]

$$S = \frac{1}{2}\langle 3\cos^2\theta - 1\rangle \qquad (1)$$

was applied to quantify the uniaxial ordering of the colloidal assembly; θ is the misfit angle of the crystal domain with respect to the colloidal line. The brackets denote an average over all of the particles in the assembly. When colloidal particles are perfectly oriented parallel to the epitaxial template, S will be equal to 1, whereas for a completely isotropic sample, S equals 0. Figure 3c shows the frequency dependence of the orientational order parameter and vacancy concentration of the resulting colloidal crystals. The high-quality oriented single colloidal crystals ($S = 1$) were obtained in the low-frequency range (400−800 Hz). When the frequency increased to the high range

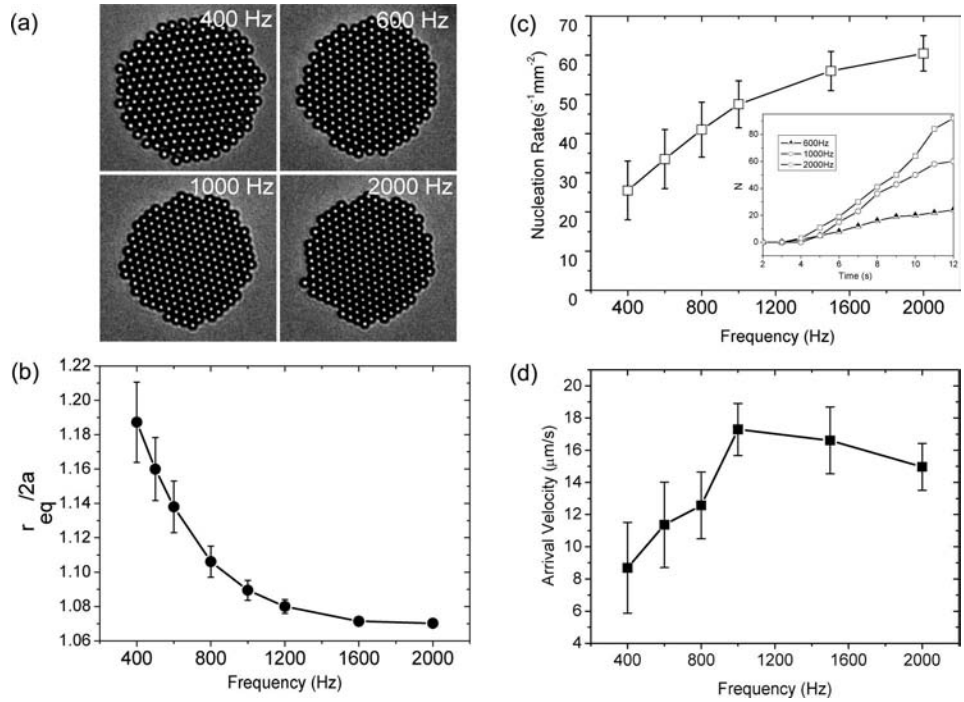

Figure 4. (a) Optical images of a colloidal assembly composed of 1.8 μm colloidal particles with different equilibrium interparticle separation, $r_{eq}/2a$, under different frequencies f on a homogeneous ITO substrate. (b) Normalized equilibrium interparticle separation, $r_{eq}/2a$, as a function of frequency f. (c) Nucleation rate as a function of frequency f. The inset shows the number of homogeneous nuclei as a function of time under different frequencies f. (d) Velocity at fixed distance of 10 μm from the template as a function of frequency f. The field strength was fixed at $E_0 = 4.0 \times 10^4$ V/m.

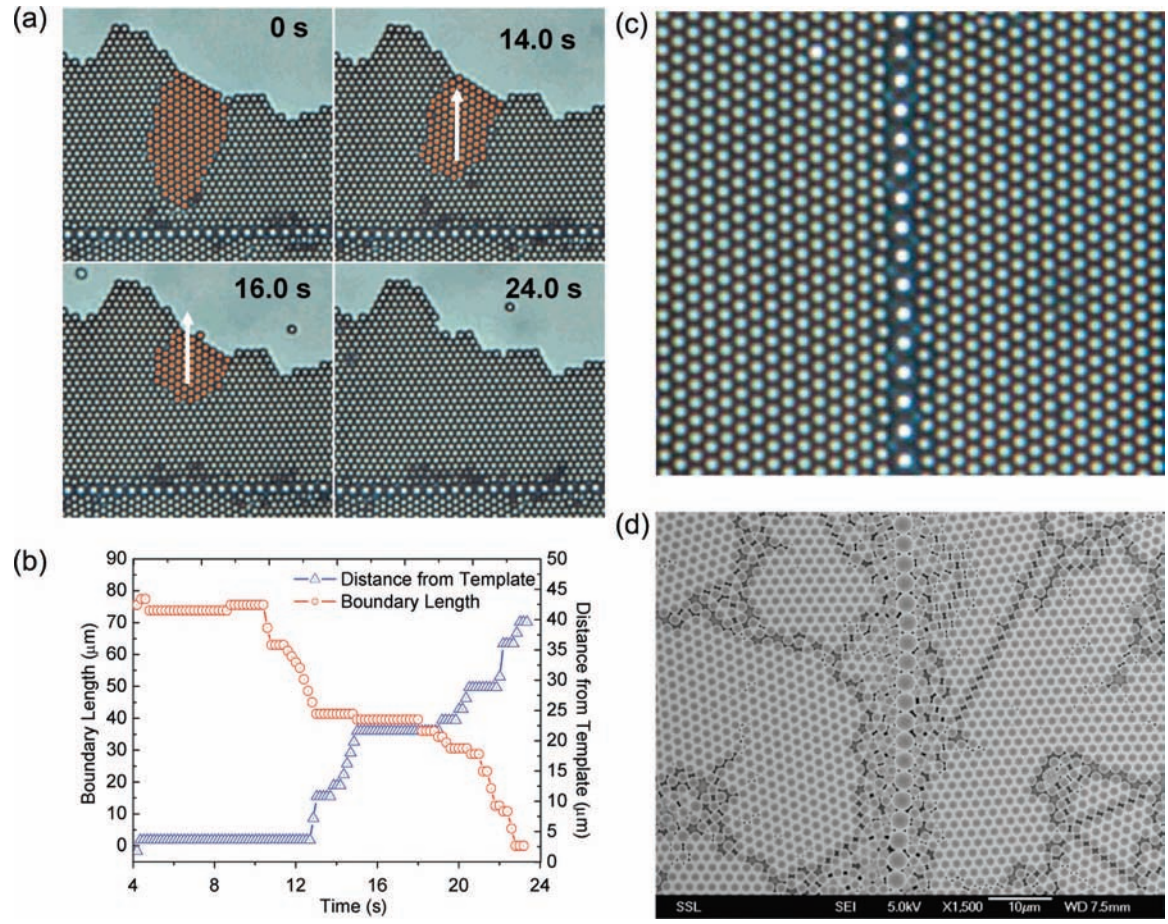

Figure 5. (a) Time evolution of a misoriented grain in a colloidal crystal composed of 1.8 μm colloidal particles and a 3.0 μm artificial linear defect, during a controllable annealing process by tuning the frequency from 1000 to 600 Hz. (b) Time evolution of boundary length and the closest distance of the misoriented grain to the template. (c) Optical image of a highly ordered colloidal crystal embedded with a linear defect obtained after the annealing process. (d) SEM image of a colloidal crystal composed of 1.8 μm colloidal particles and a 3.0 μm artificial linear defect, fabricated by a controlled evaporation method.

(1000−2000 Hz), the orientation order parameter gradually decreased, and the vacancy concentration increased ($S = 0.83$, vacancy concentration $\sim 9\%$ at $f = 2000$ Hz). This is the so-called supersaturation-driven interfacial mismatch or anti-templating effect, which has been recognized before.[37−39] The results shown in Figure 3 can be regarded as a simulation for this effect.

The correlation of frequency to the degree of perfection of the colloidal crystals can be explained in terms of the frequency-dependent interparticle interactions and the nucleation kinetics. The interparticle interactions are characterized by the equilibrium interparticle separations r_{eq} among assembly, which is determined by the competition between the EHD attractions and repulsive dipole−dipole particle interactions.[24,28−33] The EHD attractive force F_h can be approximated as Stoke's force:

$$F_h \approx 6\pi\eta a v(f,r) \tag{2}$$

where η is the viscosity of the solvent and $v(f,r)$ is the frequency-dependent fluid flow velocity at a distance r from the colloidal particles.[24] The repulsive dipole−dipole force:

$$F_e \approx 3\pi\varepsilon_0\varepsilon_s a^6 E_0^2/r^4 \tag{3}$$

is due to the instantaneous dipole moment induced in the colloidal particles subjected to an AEF, where ε_0 is the permittivity of free space and ε_s is the dielectric constant of the solvent, with $\varepsilon_s > \varepsilon_p$, the dielectric constant of the particles.[24] As shown in panels a and b of Figure 4, the interparticle separation r_{eq} among the assembly decreases with increasing frequency from 400 to 1000 Hz and then reaches its minimum in the frequency range of 1000−2000 Hz. The larger interparticle separation suggests that the repulsive dipole−dipole force is dominant in the low-frequency range (400−800 Hz), which gives rise to a lower dissociation barrier and a higher mobility of the particles. Under this condition, the interlayer transport becomes active, and the conformations and orientations of the homogeneous nuclei are readily rearranged to align parallel to the template through the DF mechanism and related ordering, leading to a high-quality single crystal ($S = 1$) with predefined orientation with respect to the template (Figure 3a). With increasing the frequency to the high range (1000−2000 Hz), the EHD attractions become more dominant, and that the particles are tightly packed ($r_{eq}/2a < 1.10$) can be inferred from Figure 4 panels a and b. The increased EHD attractions act to prevent the particles from dissociation and diffusion. When the homogeneous nuclei approached the islands, they almost kept their original conformations and orientations, resulting in the

(36) Dierking. I. *Textures of Liquid Crystals*; Wiley-VCH: Weinheim, 2003.
(37) Liu, X. Y; Sawant, P. D.; Tan, W. B.; Noor, I. B. M.; Chen, B. H. *J. Am. Chem. Soc.* **2002**, *124*, 15055–15063.
(38) Liu, X. Y.; Lim, S. W. *J. Am. Chem. Soc.* **2003**, *125*, 888–995.
(39) Li, J. L.; Liu, X. Y.; Wang, R. Y.; Xiong, Q. Y. *J. Phys. Chem. B* **2005**, *109*, 24231–24235.

formation of randomly oriented domains, boundaries, and vacancies in the resulting colloidal crystals (Figure 3b). (The direct observations of the epitaxial crystallization process and grainboundary formation at different frequencies is available as Supporting Information, Video 3.)

On the other hand, the nucleation rate (which is defined as the number of mature nuclei created per unit time per unit area, following the criteria described in ref 28) in the higher-frequency range is larger because of the increased attractions (Figure 4c). Due to an increase in the homogeneous nucleation rate, the entropy effect and the transport would result in a certain degree of randomness.[40] This would lead to a reduction of interfacial correlation between the template and the incoming growth units and thus a decrease in the degree of perfection of the colloidal crystals. The arrival rate of the growth units might affect the structure of the crystals, which was higher in the high-frequency range as well (Figure 4d). In our experiment, however, it was found that in the low-frequency range the best epitaxial correlation was maintained, even when the arrival rate was increased from 2.87 μm/s to 8.64 μm/s by increasing the field strength at 400 Hz (Figure 2c). This suggests that the arrival rate of the incoming particles is not a key parameter in controlling the degree of perfection of the resulting crystals, provided that the incoming particles maintain a high mobility at the low-frequency range.

The understanding gained here allows us to explore several important implications for practical applications accordingly. The first is the controlled engineering of defects within the colloidal crystals. To introduce well-defined linear defects inside the colloidal crystals, a colloidal line composed of 3.0 μm colloidal particles was used as template for epitaxial crystallization of 1.8 μm colloidal particles. Figure 5a shows a 1.8 μm colloidal crystal embedded with a 3.0 μm linear defect (formed under the AEF of frequency $f = 1000$ Hz and field strength $E_0 = 4.0 \times 10^4$ V/m) and its time evolution by tuning the frequency from 1000 to 600 Hz. As can be observed, there existed a misoriented domain near the colloidal line template due to lattice-mismatch (lattice mismatch: 40%)-induced disordering. Since the particle interactions can be precisely modulated by tuning the frequency of the AEF, these unwanted defects can be further eliminated through electrically induced annealing in the frequency range where the interlayer transport of colloidal particles is active. (Digital videos of electrically controlled annealing of grainboundaries are available in Supporting Information, Videos 3 and 4.) As can be seen in Figure 5, panels a and b, when the frequency was tuned from 1000 to 600 Hz, the exiting grain boundary moved away from the template, gradually shrunk with time, and then disappeared without generating new ones. Finally, a highly ordered, single colloidal crystal embedded with a well-defined artificial linear defect was obtained (Figure 5c). By contrast, the conventional evaporation method produces the colloidal crystals containing abundant lattice-mismatch-induced defects which cannot be further removed (Figure 5d). The epitaxial crystallization under the AEF shows a large accommodation of lattice mismatch of the template and a distinct advantage to relax the unwanted defects in a controllable manner, allowing the fabrication of a high-quality colloidal crystal pattern with well-defined orientations even using the poor-quality colloidal line template. The highly ordered 2D colloidal crystal embedded with a well-defined linear defect shown in Figure 5c might find application

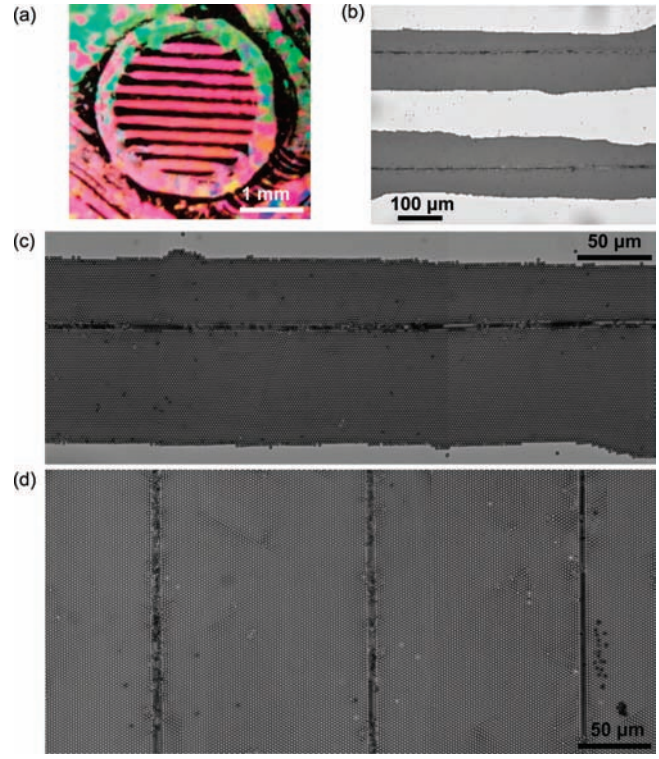

Figure 6. (a) Digital photo showing a colloidal crystal with a uniformly patterned structural color in the templated region. (b) Optical image of a typical area in the oriented patterned colloidal crystal. (c) Merged optical image showing colloidal particles aligned parallel along the colloidal line template spanning the whole length of the colloidal line. (d) Merged optical image showing large-area fabrication of a single colloidal crystal with a well-defined orientation.

as electrically tunable photonic waveguides. (Digital video of reversible tuning of lattice spacing of a colloidal crystal with artificial linear defect is available in Supporting Information, Video 5.)

The second interesting implication is the electrically switchable large-area patterning of structural color of the colloidal crystals. Figure 6a shows a digital photo of a colloidal crystal formed under the AEF of frequency $f = 800$ Hz and field strength $E_0 = 4.0 \times 10^4$ V/m, wherein a colloidal line pattern predeposited at the center region ($\sim$3 mm in diameter) was used as an epitaxial template. Due to interference of light from the long-range periodically ordered structures, this colloidal crystal pattern display iridescent structural color with respect to the crystalline orientation. As can be seen in Figure 6a, in the peripheral region without the epitaxial template, the colloidal crystal shows a colorful mosaic pattern, because the structure of the colloidal crystal is polycrystalline, consisting of grains of single crystals with randomly distributed orientations. In contrast, in the center region with a colloidal line template, the colloidal crystal shows a uniform structural color, indicating that the whole patterned region is of the same orientation. This is also confirmed by the optical images shown in Figure 6, panels b and c, wherein the colloidal particles are aligned parallel along the colloidal lines with a long-range order spanning nearly the whole length of the colloidal lines. When the AEF is switched off, the patterned structural color disappears as the colloidal crystals relax to amorphous liquid dispersion under Brownian motion. When the AEF is reapplied, the predefined structural color pattern is recovered. The reversibility of the epitaxial templating approach introduces a new class of colloidal crystals with patterns and properties that can be electrically

(40) Liu, X. Y. *J. Chem. Phys.* **1999**, *111*, 1628–1635.

switched. Such an unconventional feature will certainly add new practical applications development, such as microparticle-based displays, switchable structural color coatings, and e-papers.[19] Furthermore, by increasing the particle concentration to ensure that the whole patterned area can be fully covered with colloidal particles, a large-area (millimeter scale) single colloidal crystal with controlled orientation can be obtained. Figure 6d shows an area of a large single colloidal crystal obtained at high particle concentration (0.4%) by using an array of parallel colloidal lines with a length of 3 mm as template. The size of the single colloidal crystals can be further extended to as large as needed and is ultimately limited only by the template size.

3. Conclusion

In summary, we have demonstrated a reliable and highly efficient epitaxial templating approach to site specifically initiate 2D colloidal crystallization and precisely manipulate the kinetic growth process of 2D colloidal crystals. The interparticle interactions and, hence, the structural ordering of the resulting colloidal crystals could be conveniently tuned by changing the frequency of the AEF. This epitaxial templating approach produces highly ordered large-area colloidal crystals with controlled orientations and predefined patterns within seconds. It is particularly applicable to introduce well-defined, artificial linear defects within the colloidal crystals and to relax the unwanted existing defects in a controllable manner. Moreover, it is reversible and scalable for large-area on-chip oriented patterning. The experimental methodology adopted in this work is material general;[25] it works for biological cells, metal nanoparticles[21] as well as silica and polymer particles with sizes ranging from submicrometer to micrometer,[30] opening a wide range of applications, such as electrically tuned 2D photonic waveguides, switchable structural color coatings, and e-papers.[19]

Acknowledgment. This work was supported by ARF Projects R-144-000-148-112 and R-144-000-202-112.

Supporting Information Available: Experimental procedure, five digital videos of large-area epitaxial crystallization, defect annealing, reversible tuning of lattice spacing of colloidal crystals under AEF, digital video of freezing the colloidal crystal. This material is available free of charge via the Internet at http://pubs.acs.org.

JA900049R